Geofísica Internacional (2017) 56-4: 359-375

Original paper

Effects of the soil properties on the sea pressure profile due to seismic motions

Alejandro Rodríguez-Castellanos*, Rafael Ávila-Carrera, Ernesto Pineda-León, Víctor Martínez-Calzada and Francisco José Sánchez-Sesma

Received: October 27, 2016; accepted: August 25, 2017; published on line: October 01, 2017

Resumen

Un gran número de sismos tienen epicentros en áreas fuera de la costa y sus efectos son preocupantes. Este artículo aplica, para problemas bidimensionales, el Método Indirecto de Elementos Frontera para calcular el perfil de presiones sísmicas, en toda la profundidad del agua, debida a la incidencia de ondas P y SV sobre un fondo marino, el cual se caracteriza por su relación de Poisson. Se hace énfasis también en las amplificaciones del fondo marino. Nuestra formulación puede ser considerada como una implementación numérica del Principio de Huygens, en el cual las ondas difractadas son construidas desde las fronteras desde las cuales son radiadas. Esto es equivalente al teorema de representación de Somigliana. Los resultados numéricos muestran la importancia de las propiedades del suelo marino debido a que el perfil de presiones muestra mucha dependencia respecto a ellas. En algunos casos, las amplificaciones de las presiones son seis veces entre valores extremos del suelo. Se incluyen también, resultados de modelos con estratos y se evidencia que las amplificaciones sísmicas que pueden alcanzarse se encuentran entre 15.57 y 18.36 veces la onda incidente P y SV, respectivamente.

Palabras clave: Método Indirecto de Elementos Frontera, ondas elásticas, fondo marino, sismo marino, perfil de presiones sísmicas, relación de Poisson.

Abstract

Large number of earthquakes have epicenters in offshore areas and their effects are a matter of great concern. This paper applies, for two dimensional problems, the Indirect Boundary Element Method to calculate the seismic pressure profile with the water depth due to the incidence of P- and SV-waves on the seabed, which can be characterized using the soil properties. Moreover, seismic amplifications of the seabed are highlighted. Our formulation can be considered as a numerical implementation of the Huygens' Principle in which the diffracted waves are constructed at the boundary from which they are radiated. Thus mathematically, it is fully equivalent to the classical Somigliana's representation theorem. Numerical results show the importance of knowing the properties of the marine soil because the pressure profile has an enormous dependence with respect to them. In some cases, pressure amplifications of six times between extreme values of soil materials can be expected. In addition, results from a layered numerical model evince that large seismic amplifications may be found, they can reach values up to 15.57 and 18.36 times the incident P- and SV-waves, respectively.

Keywords: Indirect Boundary Element Method; elastic waves; seabed; seaquake, seismic pressure profile; Poisson's ratio.

A. Rodríguez-Castellanos*
R. Ávila-Carrera
Instituto Mexicano del Petróleo
Eje Central Lázaro Cárdenas 152
Gustavo A. Madero, 07730
México CDMX, México
*Corresponding author: arcastel@imp.mx

A. Rodríguez-Castellanos*
V. Martínez-Calzada
Escuela Superior de Mecánica y Eléctrica
Instituto Politécnico Nacional
Unidad Profesional Adolfo López Mateos s/n
México CDMX, México

E. Pineda-León
Escuela Superior de Ingeniería y Arquitectura
Instituto Politécnico Nacional
Unidad Profesional Adolfo López Mateos s/n
México CDMX, México

F. José Sánchez-Sesma
Instituto de Ingeniería
Universidad Nacional Autónoma de México
Ciudad Universitaria
Delegación Coyoacán, 04510
México CDMX, México

Introduction

A large number of earthquakes have epicenters in offshore areas (Mangano *et al,.* 2011). Seaquakes are characterized by the propagation of vertical earthquake motion on the sea bottom as a compressional wave and cause damage to ships, and their effect on floating structures is a matter of great concern (Takamura *et al*., 2003). When the seabed is vibrating due to a seaquake, the compressional waves propagate with the water depth due to compressibility of water.

An analytical approach that can predict the dynamic response of a flexible circular floating island subjected to seaquakes was studied by Tanaka *et al.* (1991). The floating island was modeled as an elastic circular plate, and the anchor system to be composed of tension-legs. Linear potential flow theory applied to flexible floating island subjected to wind-waves and seaquakes was presented in Hamamoto *et al.* (1991), where the hydrodynamic pressure generated on the bottom surface of the island was obtained in closed form. The nonlinear transient response of floating platforms to seaquake-induced excitation was studied by Arockiasamy *et al.* (1983), where cavitation effects were considered.

A special boundary method for earthquake-induced hydrodynamic pressures on rigid axisymmetric offshore structures, including both the water compressibility and seabed flexibility, was presented by Avilés and Li (2001). A boundary integral equation was derived assuming that the seabed is a semi-infinite homogeneous elastic solid in order to analyze the seaquake-induced hydrodynamic pressure acting on the floating structure (Takamura *et al.,* 2003). Boundary integral equations have been also used to calculate the hydrodynamic pressure caused by seaquake in layered media (Higo, 1997), and for three dimensional cases in Jang and Higo (2004). Recently, the boundary element method and the discrete wave number method have been used to determine pressures near the interface of fluid-solid models (Flores-Mendez *et al.,* 2012, Rodríguez-Castellanos *et al.,* 2011, 2014).

The Boundary Element Method (BEM) has been applied extensively to solve problems related to fluid-solid media subjected to seismic excitations. For instance, Schanz (2001) applied the BEM to study the dynamic responses of fluid-saturated semi-infinite porous continua subjected to transient excitations such as seismic waves. Moreover, irregular fluid-solid interfaces of oceanic regions or gulf areas under seismic wave propagation were analyzed in Qian and Yamanaka (2012), here important simulations of the water reverberation in the sea due to an explosive source were dealt, which show the applicability of the BEM to marine ambient. The dynamic response of a concrete gravity dam subject to ground motion and interacting with the water, foundation and bottom sediment was studied using the Boundary Element (Dominguez and Gallego, 1996). The model is able to represent continuous media with water, viscoelastic and fluid-filled pore-elastic zones. On the other hand, the dynamic response of liquid storage tank, including the hydrodynamic interactions, subjected to earthquake excitations was studied by the combinations of the boundary element and finite element methods (Hwang and Ting, 1989). Another application of BEM is focused on the seismic response of fluid-filled boreholes. In this way, in Tadeu *et al*. (2001), the BEM is used to evaluate the three-dimensional wave field caused by monopole sources in the vicinity of fluid-filled boreholes.

It is well known that Poisson´s ratio and Young´s modulus are sufficient parameters to linearly describe the stress-strain response under hysteretic conditions. In this work, a study of the sea water pressure profiles due to seismic actions of P- and SV-waves is presented. In fact, the ratio of P- to SV-wave velocities is a function of the Poisson´s ratio, only. Bowles (1988) and Wade (1996) classify the soils using its Poisson´s ratio. While, Sánchez-Sesma and Campillo (1991), Rodríguez-Castellanos *et al.* (2005) and recently Alielahi *et al.* (2015) used this criterion to characterize the soil where the wave propagation takes place. Hence, this criterion was followed as well.

This paper applies, for 2D problems in plane strain conditions, the Indirect Boundary Element Method to calculate the seismic pressure profile with the water depth due to the incidence of P- and SV- waves on the seabed (Figure 1), which is characterized by its soil properties. Wave amplifications are also highlighted. The formulation can be considered as a numerical implementation of the Huygens' Principle in which the diffracted waves are constructed at the boundary from which they are radiated. Thus, mathematically, it is fully equivalent to the classical Somigliana's representation theorem. The results are compared with those previously published. In the following paragraphs a brief explanation of the BEM applied to sea bottom subjected to seismic motions is given.

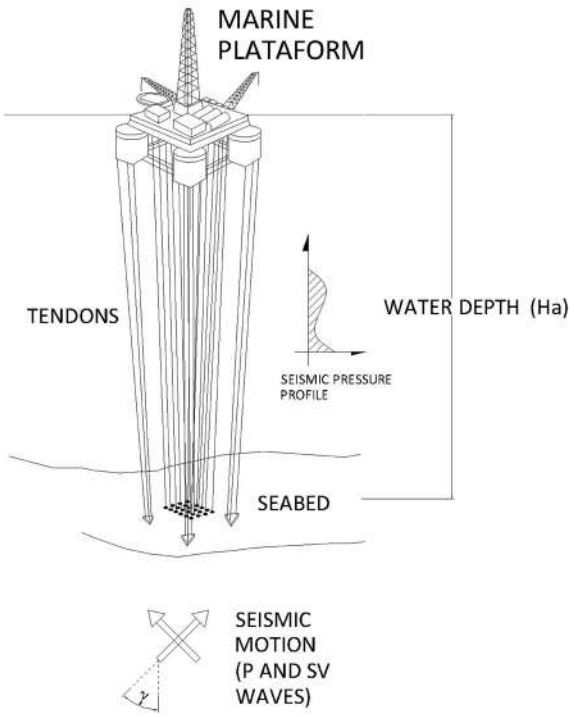

Figure 1. Marine facilities under the incidence of seismic movements.

Formulation of the method

Consider the movement of an elastic solid, homogeneous and isotropic, of volume delimited by its boundary (Figure 2), subjected to body forces $b_i(\xi, t)$ and null initial conditions. Introducing fictitious force densities $\phi_i(\xi, t)$ in Γ, the fields of displacements and tractions could be written as Banerjee and Butterfield (1981):

$$u_j(x,t) = \int_\Gamma G_{ij}(x,\xi,t) * \phi_i(\xi,t) d\Gamma_\xi + \int_\Omega G_{ij}(x,\xi,t) * b_i(\xi,t) d\Omega_\xi + u_j^o(x,t)$$
$$t_j(x,t) = \int_\Gamma T_{ij}(x,\xi,t) * \phi_i(\xi,t) d\Gamma_\xi + \int_\Omega T_{ij}(x,\xi,t) * b_i(\xi,t) d\Omega_\xi + t_j^o(x,t) \quad (1)$$

where $u_j^o(x, t)$ and $t_j^o(x, t)$ are free terms depending of the elastic wave that impinges on the body, for this research the incident P- and SV-waves propagating at some angle in a homogeneous half-space are considered. The symbol $(*)$ indicates the convolution integral in time domain, $\xi=\{x, z\}$ and $x=\{x, z\}$. $G_{ij}=\{x, \xi, t\}$ and $T_{ij}=\{x, \xi, t\}$ are Green functions for displacements and tractions, respectively. These functions are available in Rodríguez-Castellanos *et al*. (2005).

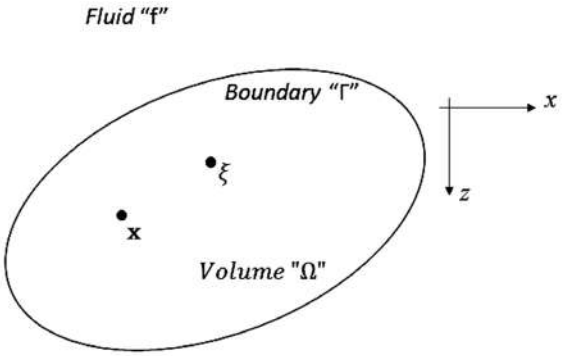

Figure 2. Elastic solid, homogeneous and isotropic, of volume Ω delimited by its boundary Γ.

For Eqs. (1), it is acceptable that these boundary integrals are valid for the main value of Cauchy. Then, if point x is allowed to approach to the boundary from inside of the region, at that time, Eqs. (1) are transformed to the next boundary equations:

$$u_j(x,t) = \int_\Gamma G_{ij}(x,\xi,t) * \phi_i(\xi,t) d\Gamma_\xi + \int_\Omega G_{ij}(x,\xi,t) * b_i(\xi,t) d\Omega_\xi + u_j^o(x,t)$$
$$t_j(x,t) = \frac{1}{2}\phi_j(x,t)\delta_{ij} + \int_\Gamma T_{ij}(x,\xi,t) * \phi_i(\xi,t) d\Gamma_\xi + \int_\Omega T_{ij}(x,\xi,t) * b_i(\xi,t) d\Omega_\xi + t_j^o(x,t) \quad (2)$$

were δ_{ij} is Kronecker´s delta.

The problem was changed to the frequency domain, accepting that the incident waves have harmonic dependency with time, of type $e^{i\omega t}$ (i.e. $u_j(x, t)= u_j(x, \omega)e^{i\omega t}$), where ω is the circular frequency and "i" is the imaginary unit. The displacements and tractions can be expressed as follow:

$$u_j(x,\omega) = \int_\Gamma G_{ij}(x,\xi,\omega)\phi_i(\xi,\omega) d\Gamma_\xi + \int_\Omega G_{ij}(x,\xi,\omega) b_i(\xi,\omega) d\Omega_\xi + u_j^o(x,\omega)$$
$$t_j(x,\omega) = \frac{1}{2}\phi_j(x,\omega)\delta_{ij} + \int_\Gamma T_{ij}(x,\xi,\omega)\phi_i(\xi,\omega) d\Gamma_\xi + \int_\Omega T_{ij}(x,\xi,\omega) b_i(\xi,\omega) d\Omega_\xi + t_j^o(x,\omega) \quad (3)$$

If the body is a fluid of volume Ω_w delimited by its boundary Γ_w then the next functions represent the displacement and pressure fields:

$$u_n^f(x,\omega) = \frac{1}{2}\psi(x,\omega) + \frac{1}{\rho\omega^2}\int_{\Gamma_W} \frac{\partial G^f(x,\xi,\omega)}{\partial n} \psi(\xi,\omega)d\Gamma_{W\xi} + \frac{1}{\rho\omega^2}\int_{\Omega_W} \frac{\partial G^f(x,\xi,\omega)}{\partial n} b^f(\xi,\omega)d\Omega_{W\xi}$$

$$pf(x,\omega) = \int_{\Gamma_W} G^f(x,\xi,\omega)\psi(\xi,\omega)d\Gamma_{W\xi} + \int_{\Omega_W} G^f(x,\xi,\omega)b^f(\xi,\omega)d\Omega_{W\xi}, \quad (4)$$

where $\psi(x, \omega)$ is the force density of fluid, ρ is the fluid density, $G^f(x, \xi, \omega)$ is the Green function for fluid pressure and is given by $Gf(x, \xi, \omega)=(\rho\omega^2)/4i\, H_0^{(2)}(\omega r/c^f)$, $H_0^{(2)}$ is the Hankel´s function of second kind and zero order, r is the distance between x and ξ, and c^f is the velocity in the fluid. The super index f denotes the fluid.

The boundary conditions of the problem, according to Figure 1, are:

On the free water surface, the pressure is null, it means:

$$p^f(x,\omega) = 0. \quad (5)$$

Onthe seabed:

Continuity of normal displacement:

$$u_i(x,\omega)n_i = u_n^f(x,\omega). \quad (6)$$

Null shear in solid-water interface:

$$(\delta_{ij} - n_i n_j)t_j(x,\omega) = 0. \quad (7)$$

The tractions on the solid are balanced with water´s pressures

$$t_i(x,\omega)n_i = -p^f(x,\omega), \quad (8)$$

where n_i is the unit normal vector associated to direction "i", $u_n^f(x, \omega)$ is the normal displacement with respect to surface of interface and $u^f(x, \omega)$ is the water pressure.

If the boundary conditions, Eqs. (5)-(8) are expressed, using the integral representations, Eqs. (3) and (4), neglecting the body forces, and if the boundaries (Γ and Γ_w) are discretized in Nel boundary elements, then the following system, known as Fredholm´s system of integral equations of second kind and zero order is found.

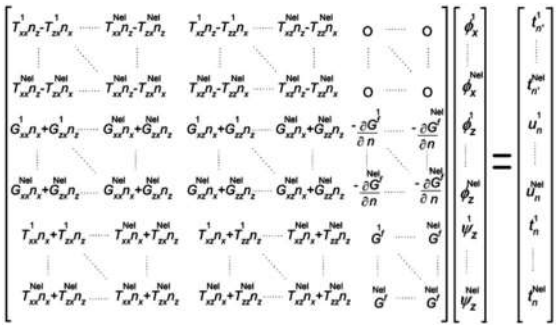

Once the solution of equation (9) is obtained, the displacement and pressure fields of equations (3) and (4), respectively, can be calculated. Additional details on the treatment to obtain the system of integral equations (9) can be consulted in Rodríguez-Castellanos *et al*. (2014).

Verification of the method and numerical examples

Verification

Wong (1982) and Kawase (1988) reported the seismic amplifications for the case of a topography with semicircular canyon shape of radius "a" (Figure 3d). They considered an elastic solid medium (with the properties shown in Table 1) in contact with an acoustic (vacuum) medium showing seismic amplifications in the solid surface between $-2 \le \frac{x}{a} \le 2$, for a frequency of $n = \frac{\omega a}{\pi\beta} = 2$. The incidence of seismic waves are P- and SV- waves with incident angles γ=0º and γ=30º, for each one.

In the present formulation, it is possible to consider that the high of the acoustic medium is approaching to infinity ($H_a \longrightarrow \infty$) (and such properties are from the air (Table 1). H_a is the water depth. Moreover, this method can deal with a solid-vacuum interface; the same problem studied by Wong (1982) and Kawase (1988) will be exactly resolved in the present study. The obtained results for the acoustic (air or vacuum) medium in contact with a solid one are displayed in Figures 3 and 4. The receivers are located on the seabed. Circles represent results by Wong and squares by Kawase. The present results are plotted with lines. In general, it is possible to appreciate a good match between the results found with the current formulation and those from the mentioned references, for both displacements and P- and SV-wave incidences.

Table 1. Elastic properties for elastic and acoustic media.

	$\alpha\left(\frac{m}{s}\right)$	$\beta\left(\frac{m}{s}\right)$	$\rho\left(\frac{m}{m^3}\right)$	Observations
Air Bedford and Drumheller (1994)	330	------	1.29	only for Verification
Elastic medium Wong (1982) and Kawase (1988)	1998	1000	2500	only for Verification

The use of the Green's functions for infinite spaces, expressed in terms of Hankel's functions of second kind, is an advantage of our integral formulation. Green's functions for a half space can be also used in problems where a free surface is present. However, these functions are more complex than those for the infinite space and do not represent substantial save in computational requirements. On the other hand, we only modeled a finite part of the water and interface. Such truncation induces artificial perturbations caused by diffractions at the edges of the numerical model. However, these perturbations are characterized by small amplitudes and their reflections inside the model are negligible. The simplest solution is to choose a surface length large enough that the fictitious perturbations fall outside the observational space-time window. Then, edge effects due to the finite size of the discretized boundaries can be neglected; therefore, absorbing boundaries are not required.

The use of dimensionless frequencies has been usually employed to express the displacement fields of soil structures under seismic motions. In this context, several authors have used dimensionless frequencies to calculate strong ground motions or surface motions due to seismic movements. For instance, Trifunac (1973) (η=0.0 to 3.0), Wong (1982) (η=0.5,1.0,1.5,2.0), Sánchez-Sesma and Campillo (1991) (η=0.0 to 4.0), Rodríguez-Castellanos *et al.* (2005) (η=0.0 to

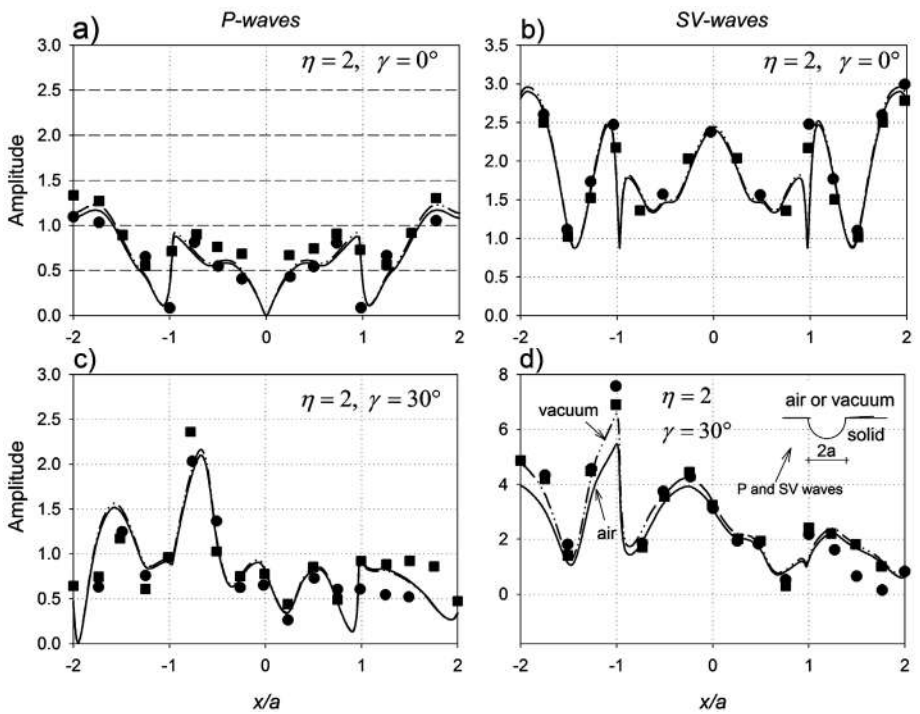

Figure 3. Comparison of results obtained by Wong (1982) (circles), Kawase (1988) (squares) and current formulation by BEM (lines). Solid line shows displacements in the x-direction for an air acoustic medium, while dash-dot-dot line shows displacements for a vacuum one.

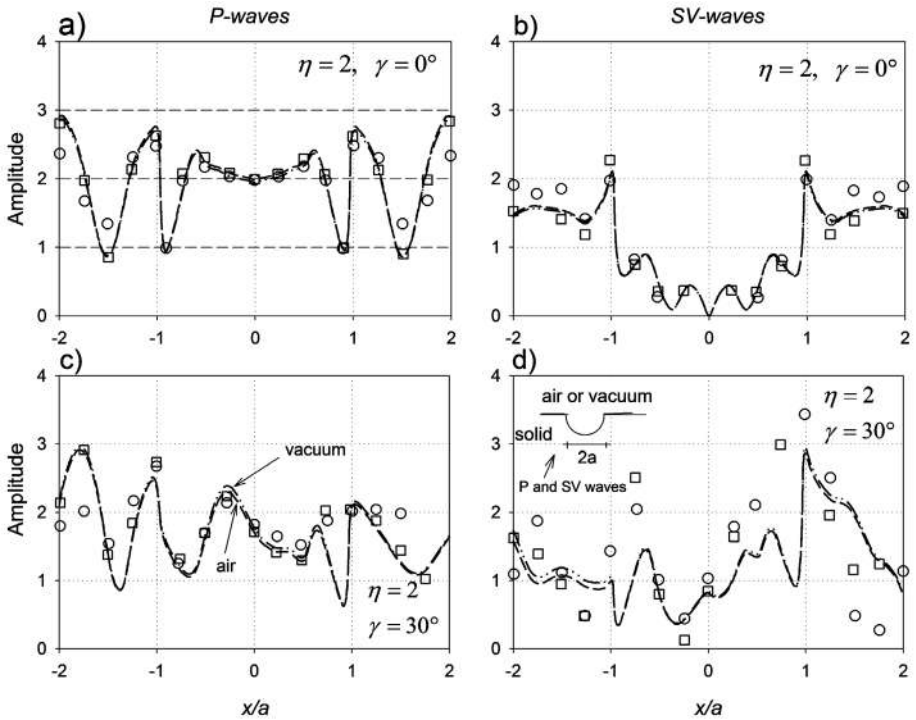

Figure 4. Comparison of results obtained by Wong (1982) (circles), Kawase (1988) (squares) and current formulation by BEM (lines). The striped line represents displacements in *z*-direction for an air acoustic medium, while dash-dot-dot line shows displacements for a vacuum one.

3.0) and recently Alielahi *et al.* (2015) (η=0.5, 1.0) used this criterion. In this work, results using η=0.0 to 4.0 are presented, this interval can be considered within the range of interest in earthquake engineering and seismology.

Numerical Examples

In order to develop numerical examples and show the influence that soil properties have on the propagation of compressional and shear waves that affect the sea bottom, and subsequently in pressure states with the water depth, the following elastic parameters were used for the analyses (see Table 2).

The pressure profiles show many different behaviors that depend mainly on the soil properties and the type of incident wave. For example, in Material 1, a lower amplification of pressures due to P-wave incidence is obtained, compared with the amplification obtained for Material 5 (see Figure 5). In Figure 5, the pressure profiles for the non-dimensional frequency of $n = \dfrac{\omega a}{\pi\beta} = 2$ and Materials 1 to 5. In Figure 5a, the pressure obtained for Material 5 is 10 times higher than the one obtained for Material 1. This effect decreases as the incident angle of P- wave increases (i.e. γ=60º). For all cases presented in this figure, the condition of zero pressure in the water surface is satisfied. In general, the incident SV-waves produces less pressure than that obtained for P-waves. In Figure 5b, it is verified that SV-wave with normal incident (γ=0º) does not generate any pressures state, for any material. Figure 5f indicates that a marine soil of Material 1 produces an oscillatory behavior with water depth. In most of the studied cases, the maximum pressure obtained is near the seabed; this is important to be considered for the design of facilities attached on the seabed.

For Material 1, the underlying solid pressure variation with the water depth shows relatively small values for P-wave incidences with the three selected angles (0, 30 and 60 degrees) because of the impedance contrast between solid and fluid. On the other hand, for incoming SV-waves and large incidence angle (60 degrees) the horizontal phase velocity is quite large, as compared with the propagation velocity within the fluid. This and the polarization of motion induce significant emission of waves within the solid for a quasi- vertical direction.

Table 2. Parameters used for analyses

Elastic medium	SV-wave velocity (β) (m/sec)	Density (ρ) (kg/m^3)	Poisson's ratio (υ)	Reference
1	3000	2100	0.25	
2	400	1700	0.35	Huerta-Lopez *et al*.
3	190	1400	0.40	2003 and 2005
4	90	1300	0.45	
5	20	1320	0.495	Roever *et al*., 1959

Figure 6 depicts the behavior of pressures when P- and SV-waves impact a sinusoidal bathymetry (see detail in Figure 6f). The material properties and incident angles of the elastic waves are the same as in Figure 5. For the case of P-waves, the pressure field shows small variations in comparison with a flat interface. However, for the case of SV-waves, diffracted pressure waves are present for an incident angle γ=0º. For angles of γ=30º and γ=60º the pressures describe patterns similar to those for a flat interface (Figure 5), but they reach lower values.

Figure 7 shows the pressure fields obtained at several water depths. These pressures were calculated at six locations (H/H_a=0, -0.20, -0.40, -0.60, -0.80 and -1.0) for a frequency range of $0<\eta<4.0$. The soil has the properties of Material 1, according to Table 2. In this case, normal (γ=0°) and oblique (γ=30°) P- and SV-wave incidences on a flat interface (Figure 7a) are considered. It must be emphasized that for all the cases null pressures are obtained on the water surface (Figures 7b-e), as expected. On the other hand, null pressures are obtained, when an SV-wave impacts with an angle γ=30°

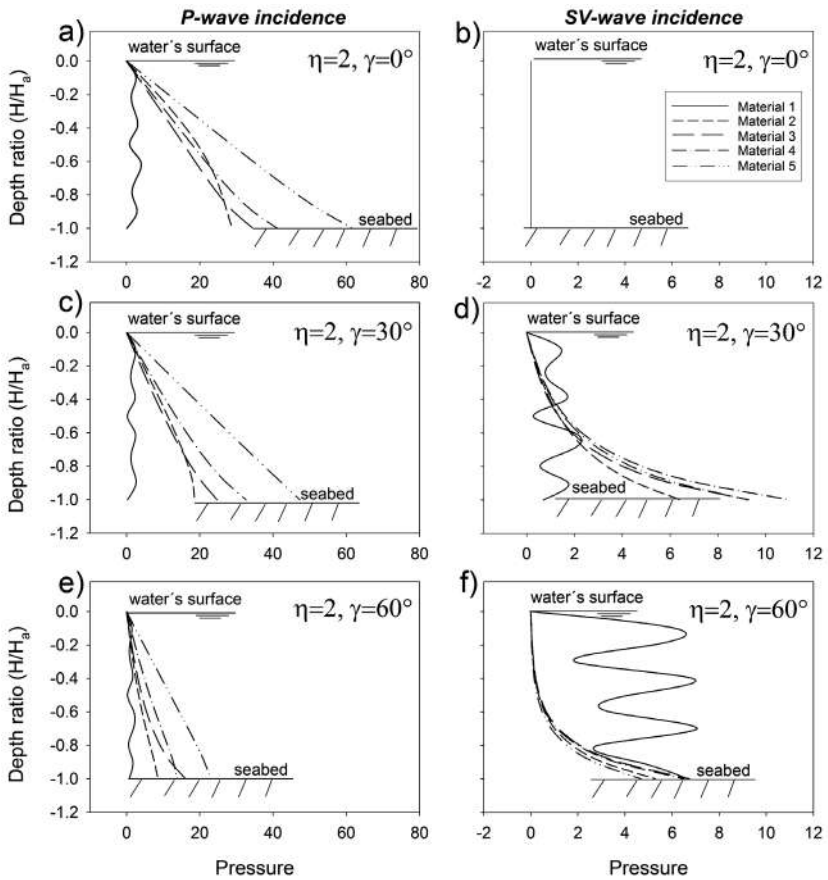

Figure 5. Pressure spectrum for different soil properties of seabed and incident angle of P- and SV-waves, for a flat bathymetry.

(Figures 7c, g, k, o, s, and w). It can also be said that several peaks are present in the graphs, which are associated with the resonances generated by waves interacting between the water surface and the seafloor. These peaks appear clearly in the case of normal P-wave incidence and near to the seafloor (H/H_a = -1.0, Figure 7v). In addition, it is noticeable that the oblique P- and SV-wave incidences (γ= 30°) generate pressure fields at the six mentioned locations. However, these pressures show less amplitude than those generated by a normal P-wave incidence. In general terms, the greatest pressures are present in the proximity of the seafloor (Figures 7v, x and z), which have been also highlighted in the previous analyzes.

Figure 8 displays the propagation of P-waves calculated in 51 receivers spaced 0.04 H/H_a. The propagation is presented for five types of seabed, according to Table 2, for Materials 1 to 5. The first 25 receivers are located in the solid, see bottom figures showing displacements in the z-direction. Displacements for the x-direction are zero when a normal P-wave impacts the interface. The last 26 receivers are located in the water, see top figures showing the pressure generated by the incidence of P-waves. A normal incidence (γ=0°) of P-waves that impinges on a flat and horizontal surface does not create diffraction in the x-direction. In general terms, an incident wave that is propagating in the solid is transmitted to the fluid generating a pressure field. It can also be seen that the water surface causes the reflection of waves that propagate in the opposite direction. Later, in Figure 10 pressures obtained nearby seabed are discussed.

In Figure 8, the displacements for 64 frequencies up to 15.39 Hz at the mentioned receivers were computed in the frequency domain. In order to simulate the motion with the time we used the FFT algorithm to calculate synthetic seismograms using a Ricker wavelet. This pulse has a temporal dependence given by:

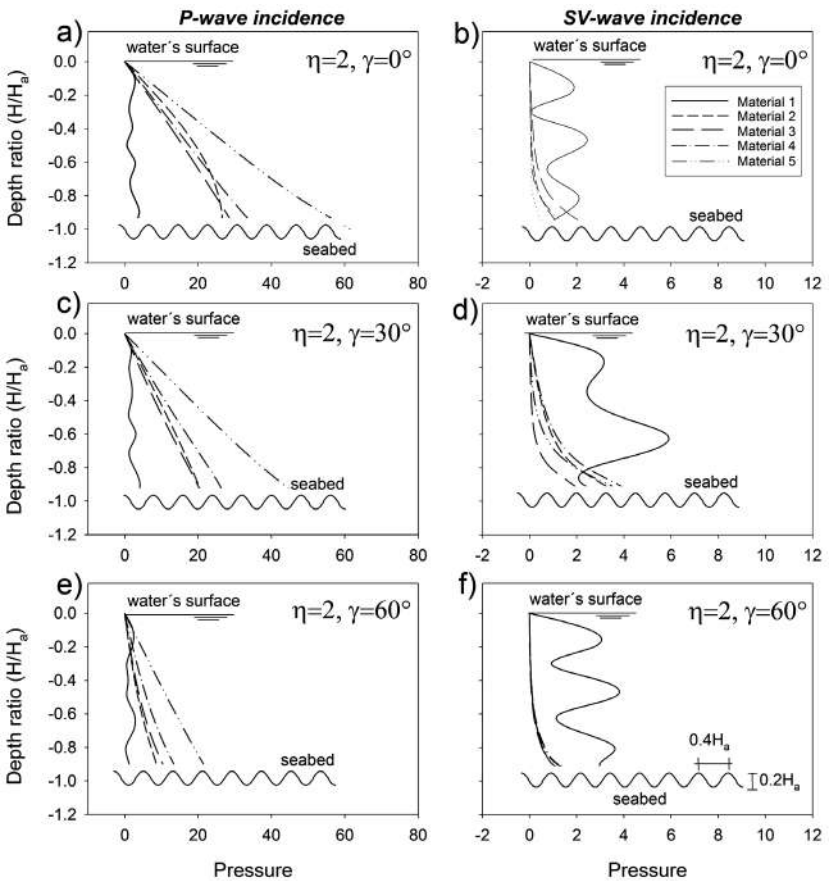

Figure 6. Pressure spectrum for different soil properties of seabed and incident angle of P- and SV-waves, for a sinusoidal bathymetry.

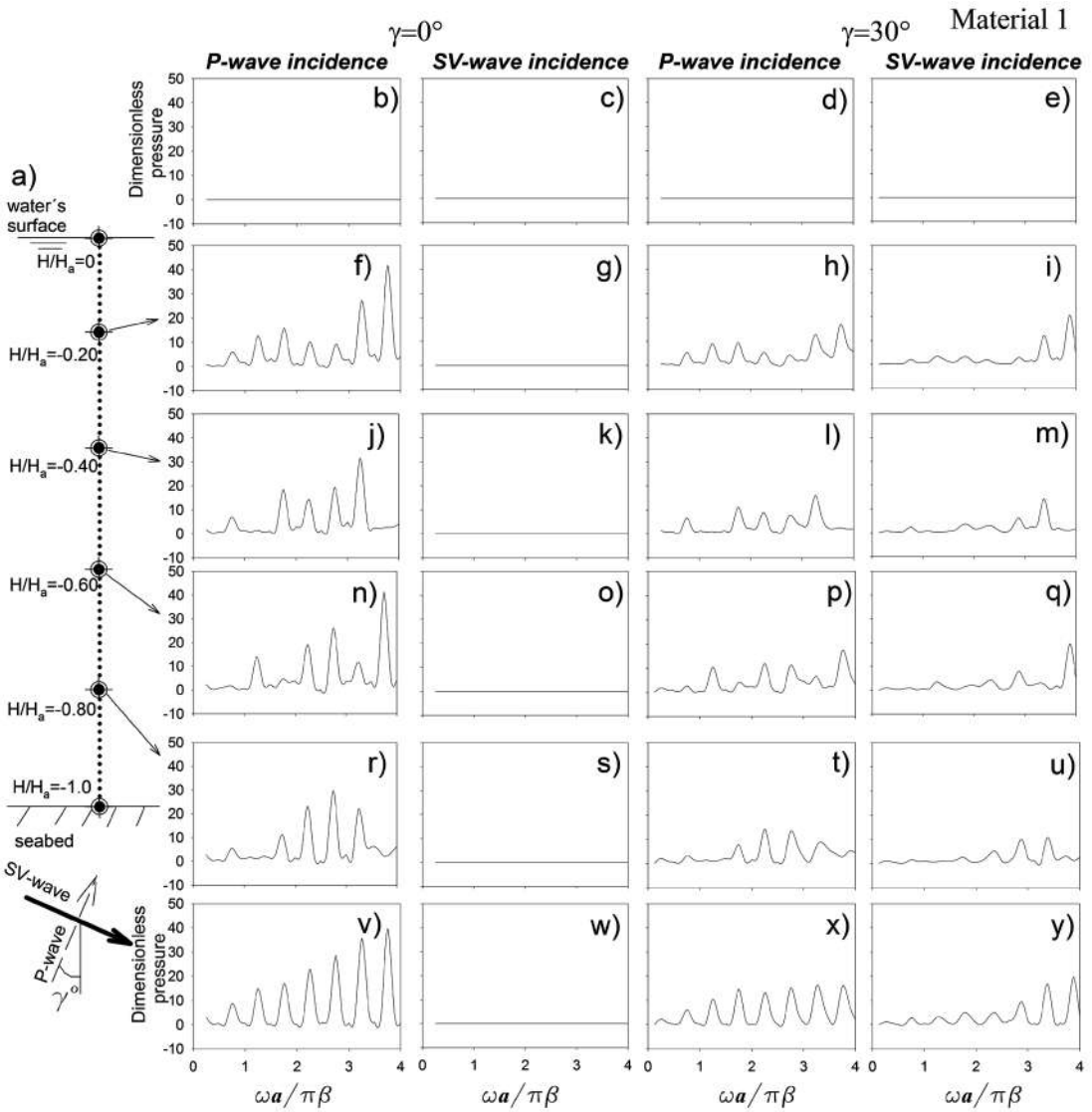

Figure 7. Pressure spectrum at several water depths. The range of dimensionless frequency is $0<\eta<4.0$.

$$R(t) = a(t) - \frac{1}{2} e^{-a(t)}, \qquad (14)$$

where

$$a(t) = \frac{(t - t_S)}{t_p}^2, \qquad (15)$$

t_p = characteristic period, and t_s = time-lag or offset. In the present computations t_p = 0.259 sec and t_s = 0.779 sec were used. The time scale is given by $\beta t/H_a$ (normalized time).

Physically, η represents the ratio of the water depth (H_a) to the incident wavelength. The range of frequency (64 frequencies up to 15.39 Hz) permits to generate a Ricker pulse with a wavelength that can "feel" the interface and the water surface. According to this, Figure 8 makes clear that several wave diffractions and reflections take place in the water, for the selected wavelength.

In Figure 8, the incidence of elastic waves on the interface produces the phenomenon of reflection and refraction of waves and also the appearance of interface waves (Scholte

waves). This last type of wave appears once the interface is excited. The energy that carries this wave dissipates during its travel, radiating energy towards the fluid and the solid medium. In Figures 8a-j, the interface waves continue to radiate energy and generate variations in pressure after the first reflections and refractions have taken place. These pressure variations can be seen from 1.7 to 2 seconds for the case of Figure 8a, from 1.5 to 1.7 seconds in Figure 8b, from 1.3 to 1.8 seconds in Figure 8c and from 1 to 1.5 seconds in Figure 8d. In all these cases, the influence of the Poisson ratio on the pressure state in the fluid can be observed. A detailed study of the interface waves and their effect on pressure can be found in Borejko (2006).

The incidence of P- and SV-waves on the seabed could cause displacements in x and z-directions. The calculated amplitudes are dependent on the type of the seabed material and the incident angle of the seismic movements. Figure 9 shows the displacements produced in the seabed at frequency η=2 for incident P- and SV-waves at angles=0º, 30° and 60°. Materials 1 to 5 were analyzed. In general terms, the normal incidence of P-waves causes amplitudes of vertical displacement (z) close to 3 (Figure 9c). For other angles of incidence the displacement is lower. The normal incidence of SV-waves gives zero displacements in the vertical direction (Figure 9d), while for other angles of incidence such displacements are small compared to those caused by P-waves. The maximum displacement in the x-direction is produced by the normal incidence of SV-waves, these displacements decrease as the incidence angle increases. The diffraction caused by P-waves is very small for the incidences and 30°, whereas for γ=60º it reaches a value near to 2 for Material 1.

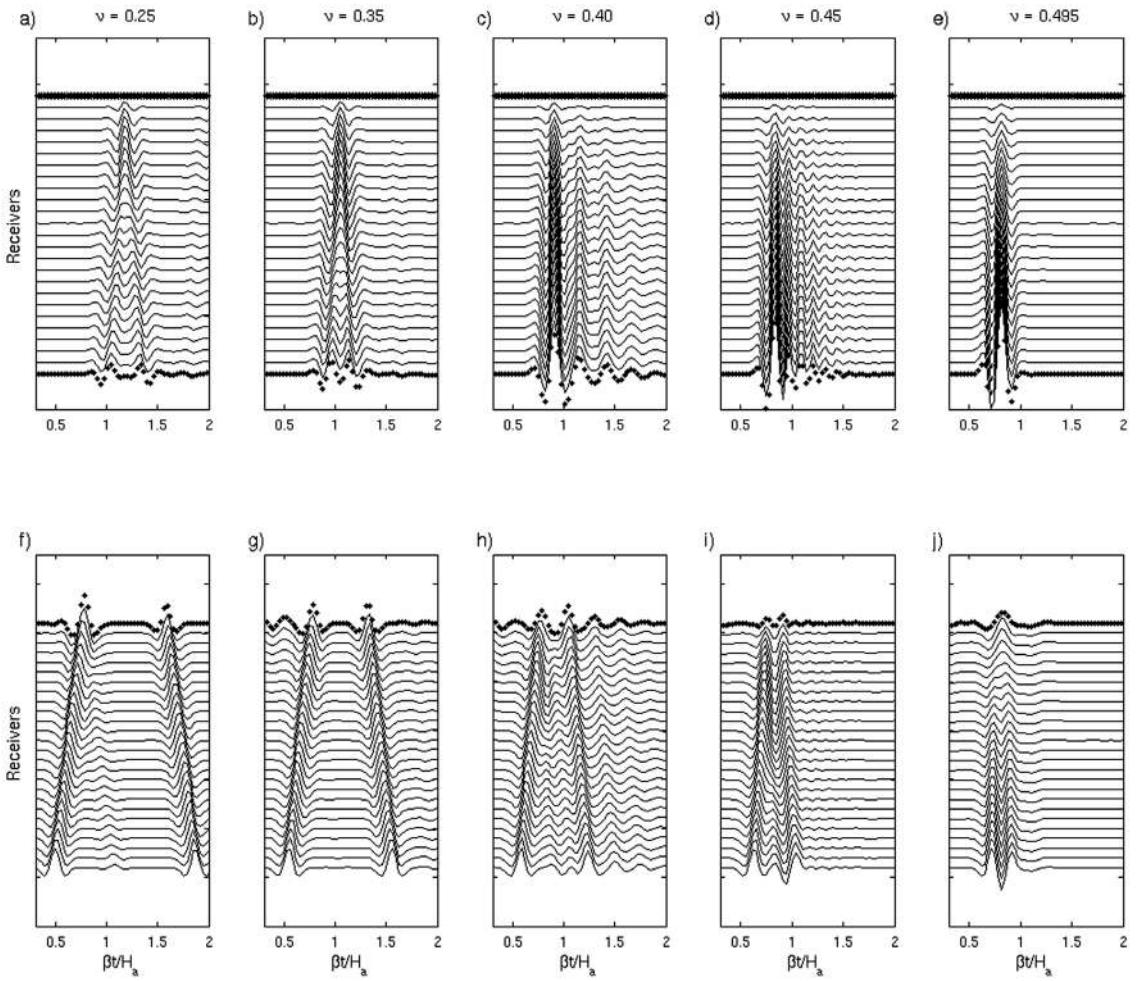

Figure 8. Propagation of compressional waves recorded at 51 receivers for different materials: water pressure (top figures) and displacement in z-direction in the solid (bottom figures).

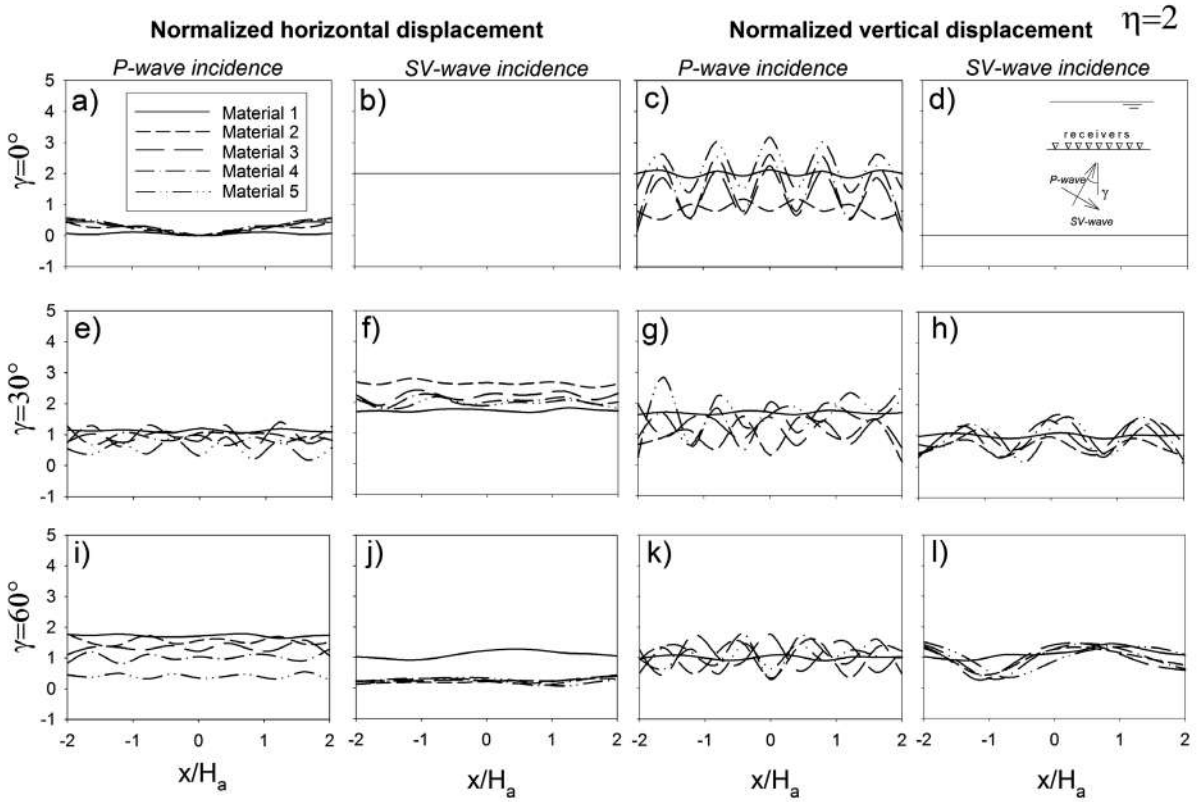

Figure 9. Displacement amplitudes calculated on seabed resulting from incidence of P- and SV-waves with angles of γ=0°, 30° and 60°.

Figure 10 presents the pressures in time domain, obtained in the vicinity of the seabed for Materials 1 to 5 and for normal incidence of P-waves. It is clear that for Material 5 strong amplifications in the range of 6.05 times are obtained in comparison with Material 1 (see Figure 10e). This result shows the importance of adequately characterizing the type of soil where marine structures will be located since strong amplifications of seaquakes can be present.

Now, results for a layered medium are displayed. This medium is composed of an elastic half space (Material 1), a layer (Material 2) and the sea water. The elastic properties of the solid medium can be found in Table 2. The studied model is detailed on Figure 11e, where the localization of receivers 1 and 2 are also shown. Receiver 1 is located on the seafloor and receiver 2 is between the two solid materials. We studied two layer thicknesses, one of h/H_a=0.025 (Figures 11c and d) and another of h/H_a=0.05 (Figures 11a and b). These figures show the calculated seismic amplifications in such receivers for a frequency range $0<\eta<4.0$. For this purpose, the normal incidence (γ=0°) of P- and SV-waves on the stratified medium (Figure 11e) is considered. In this figure, it is remarkable that the greatest seismic amplifications are obtained at Receiver 1, reaching a value of 15.57 for the incidence of P-waves (Figure 11a) and 18.36 (Figure 11b) for SV-waves. These values correspond to the case of a layer thickness of h/H_a=0.05. In fact, in this case, the layer with greater thickness generates larger seismic amplifications with respect to the layer of reduced thickness. In the case of h/H_a=0.025, the maximum amplifications obtained correspond to 11.08 (Figure 11c) for the incidence of P-waves and 16.25 (Figure 11d) for SV-waves. In addition, the presence of the layer causes more oscillations in the response associated with the P- waves, in comparison to the SV-waves. Such interactions generate sharp peaks in the response obtained. It should be noted that in all cases, the displacements calculated for the receiver 2 had an average value of 2. Strong amplifications by soft layer have been previously reported in the field of earthquake engineering and seismology. For example,

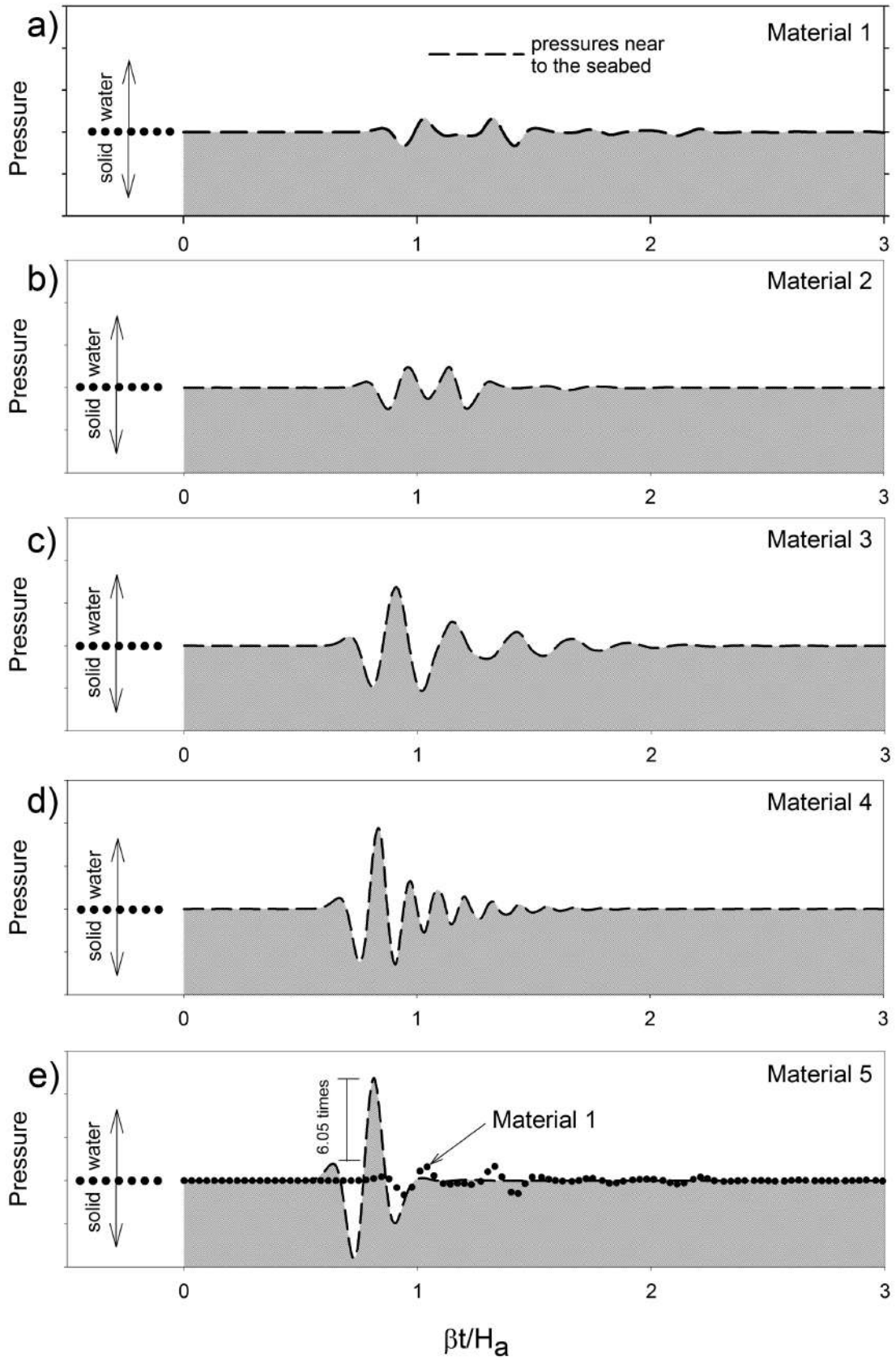

Figure 10. Maximum pressures calculated nearby the seabed for Materials 1 to 5, for normal incidence of P- waves.

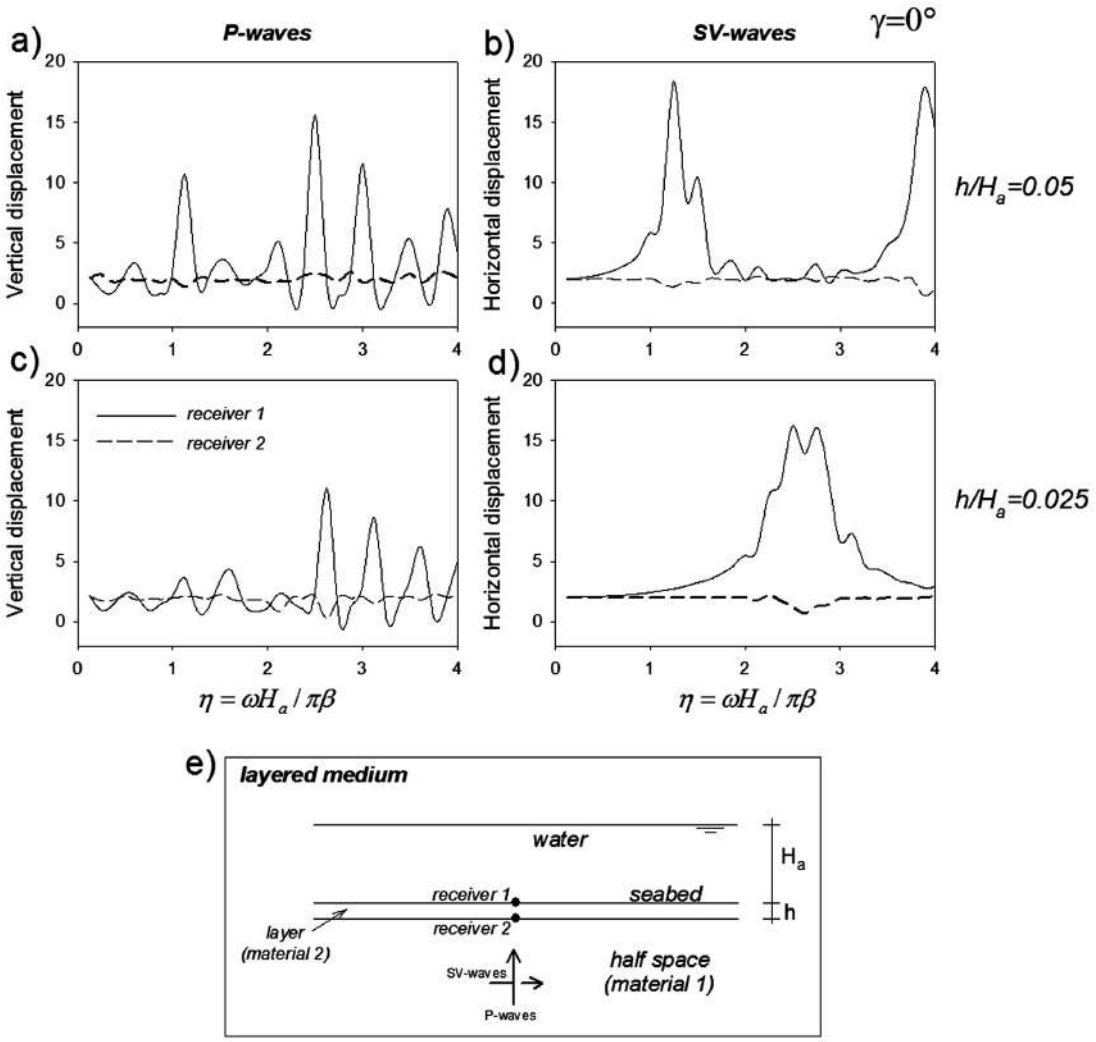

Figure 11. Vertical and horizontal amplifications due to the normal incidence of P- and SV-waves on a layered medium. The range of dimensionless frequency is $0<\eta<4.0$.

one of the first contributions on seismic amplifications is that of Trifunac (1971), where he showed amplifications around 20 times the incident wave, for the case of an SH-wave hitting an alluvial valley. It should be mentioned that the normal incidence of P- and SV-waves does not cause displacements in the horizontal and vertical direction, respectively. It is important to emphasize that the presence of a soft layer can generate large seismic amplifications, which must be taken into account in the design of marine installations.

In the case of an oblique incidence of elastic waves (P and SV), seismic amplifications are present for both components of displacement. Such amplifications can reach considerable values. Then, considering the models and materials of Figure 11, and hitting the medium with an incident angle of elastic waves of γ=30º, the seismic amplifications reach large values. For example, Figure 12c exhibits an amplification of 15.68 (at a frequency of η=3.62), which corresponds to the case of h/H_a=0.025 under the incidence of P-waves. On the other hand, the incidence of SV-waves generates amplifications of 15.11 (Figure 12h), which also corresponds to the case of h/H_a=0.025. This figure makes it clear that the oblique incidence of elastic waves can generate high seismic amplifications, for both components of displacement, although these amplifications are smaller than those obtained in the case of the normal incidence (γ=30º, Figure 11). It should be noted that Receiver 1 is again the one that reaches the largest seismic magnifications.

Finally, with the purpose of illustrating the effect that the presence of a layer has on the pressure field in the water, Figure 13 is included. Again, the models and materials used for the previous simulations were considered. But now the frequency of η=3.62 has been selected, which corresponds to the frequency where the greater amplification for previous case was obtained (Figure 12c). To display the pressure field in the water, three incident angles of elastic waves (γ=0º, 30° and 60°) were selected. The layer is formed by Material

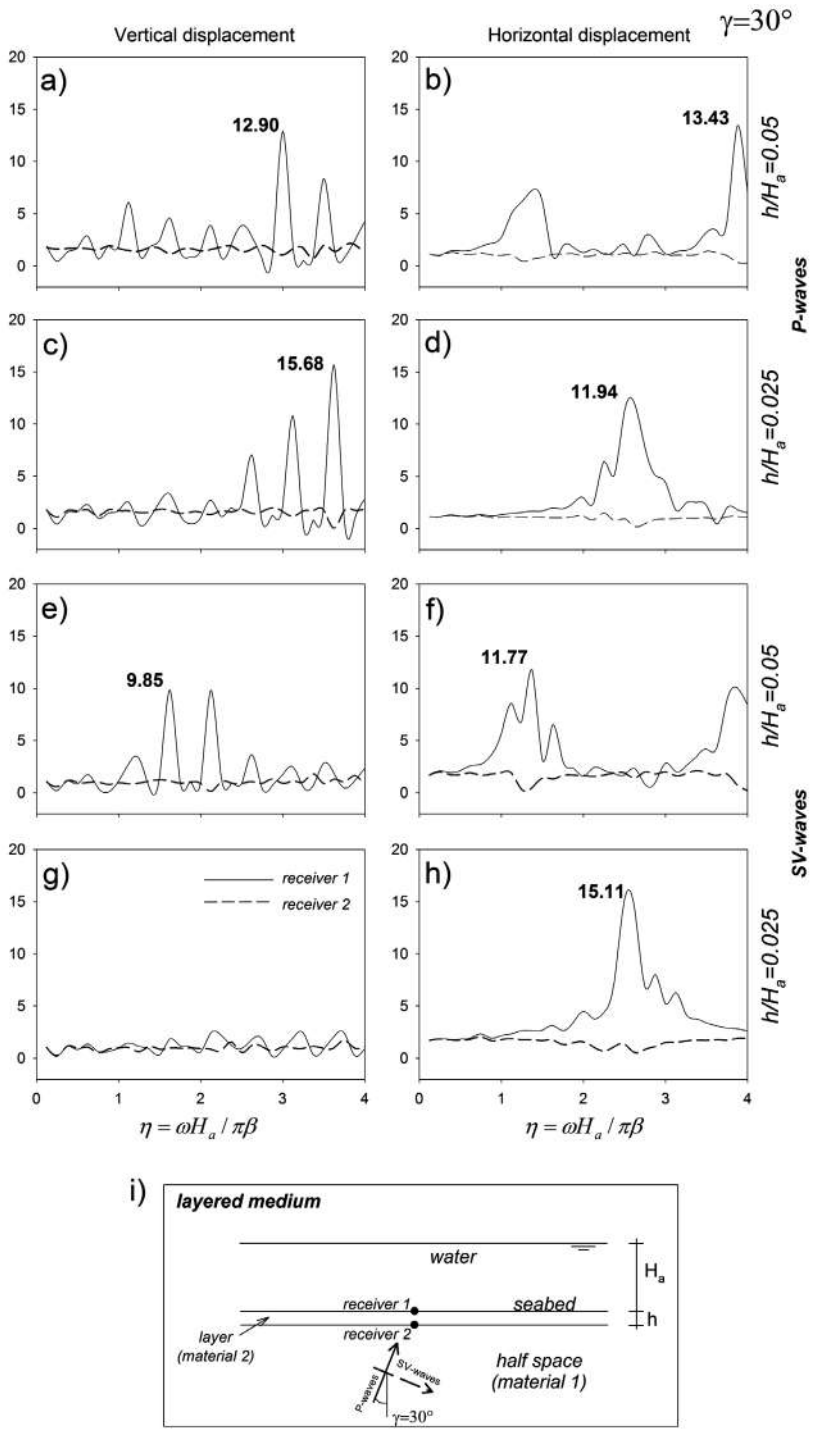

Figure 12. Vertical and horizontal amplifications due to the oblique incidence of P- and SV-waves on a layered medium. The range of dimensionless frequency is 0<η<4.0.

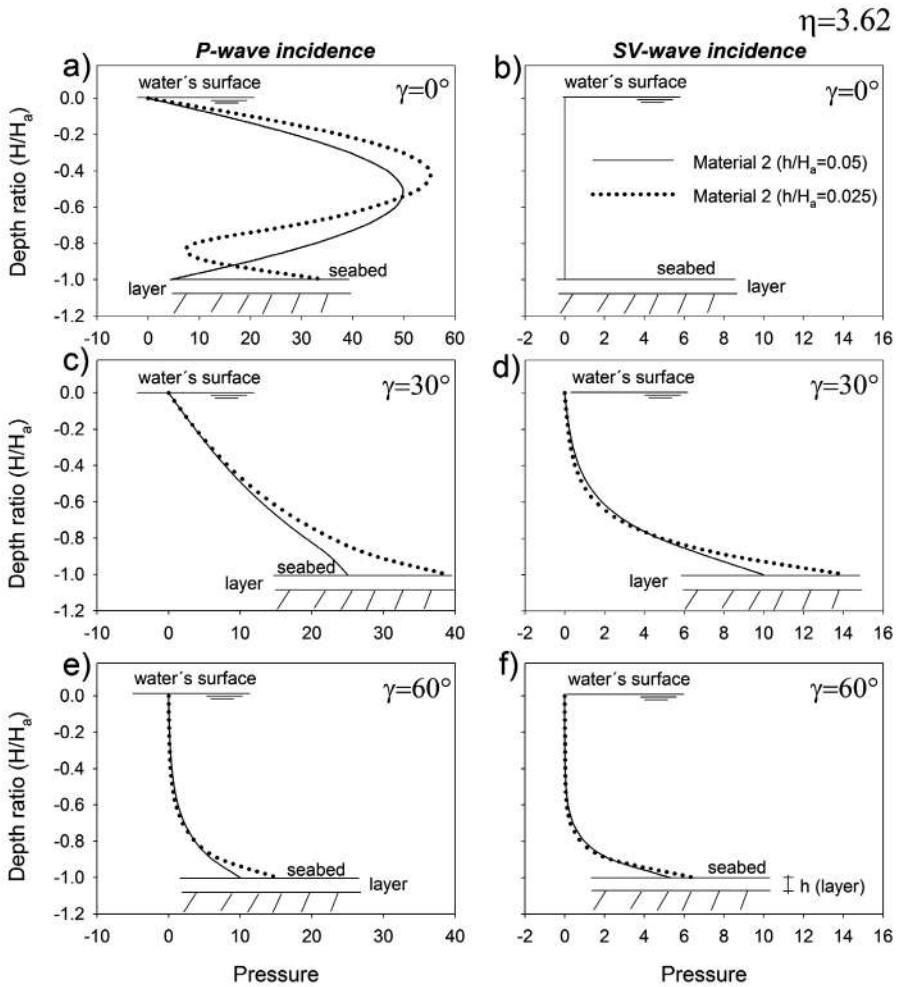

Figure 13. Pressure spectrum for layered media with various incident angles of P- and SV-waves.

2 and its thickness is given by h/H_a=0.025 and 0.05. The pressure field for the thinner layer is graphed with a dotted line, while for the thick layer a continuous line is used (Figure 13b). It should be noted that the presence of the layer causes variations in the pressures calculated throughout the water depth and mainly in the proximity of the sea bottom. It is important to emphasize that for these cases and for the frequency studied (η=3.62) greater pressures are achieved for the case of h/H_a=0.025. This result is more evident for the incidence of P- and SV-waves with an incident angle of γ=30º (Figures 13c and d). On the other hand, the incidence of SV-waves with γ=0º does not generate pressure fields in the water (Figure 13b). For the incidence of elastic waves with an angle of γ=60º, the pressure field practically remains unchanged, for both layer thicknesses.

Conclusions

This paper applies the Indirect Boundary Element Method to calculate the seismic pressure profile with the water depth due to the incidence of P- and SV-waves on the seabed. Two dimensional problems, in plane strain conditions, are considered. This formulation can be considered as a numerical implementation of the Huygens' Principle in which the diffracted waves are constructed at the boundary from which they are radiated. Thus, mathematically it is fully equivalent to the classical Somigliana's representation theorem. The results suggest that the pressure profile shows very different behaviors that depend mainly on the soil properties and the type of incident wave. Overall, the incidence of SV-waves produces a less pressure magnitude than that obtained for P-waves. In most cases

studied, the maximum pressure obtained is located nearby the seabed. This is important for the design of facilities supported on the seabed. Moreover, it has been shown that for a soil type of Material 5, seismic amplifications on the seabed are 6.05 times larger than those obtained for Material 1. Furthermore, results from the layered numerical model evidence that large seismic amplifications may be found, reaching values up to 15.57 and 18.36 times the incident P-and SV-wave, respectively. These results demonstrate the importance of adequately characterizing the type of soil where marine structures will be located.

Acknowledgments

Thanks are given to Dr. J. Efraín Rodríguez Sánchez for his useful revisions and comments, and to Instituto Mexicano del Petróleo – SENER-CONACYT Shale Gas/Oil Proyect (Y.60021).

References

Alielahi H., Kamalian M., Adampira M., 2015, Seismic ground amplification by unlined tunnels subjected to vertically propagating SV and P waves using BEM, *Soil Dyn. Earthq. Eng.*, 71, 63-79

Arockiasamy M., Munaswamy K., Swamidas A.S.J., Reddy D.V., 1983, Response of floating platforms to seismic excitation, *Eng. Anal.*, 1, 54-60.

Avilés J., Li X., 2001, Hydrodynamic pressures on axisymmetric offshore structures considering seabed flexibility, *Comput. Struct.*, 79, 2595-2606.

Banerjee P.K., Butterfield R., 1981, *Boundary Element Methods in engineering science*, Mc.Graw Hill. London.

Bedford A., Drumheller D.S., 1994, *Introduction to elastic wave propagation*, John Wiley & Sons, Chichester.

Borejko P., 2006, A new benchmark solution for the problem of water-covered geophysical bottom, *International Symposium on Mechanical Waves in Solids, Zhejiang University, Hangzhou, China,* 15-16 may 2006.

Bowles J.E., 1988, *Foundation analysis and design*, McGraw Hill, fourth edition, New York.

Dominguez J., Gallego R., 1996, Earthquake response of gravity dams including effects of porous sediments, *Proceedings of Engineering Mechanics, 2, 649-652, 1996; Conference: Proceedings of the 1996 11th Conference on Engineering Mechanics. Part 1 (of 2), May 19, 1996 - May 22, 1996; Sponsor: ASCE; Publisher: ASCE*.

Flores-Mendez E., Carbajal-Romero M., Ortiz-Alemán C., Rodríguez-Sánchez J.E., Rodríguez-Castellanos A., 2012, Modeling of fluid-solid interfaces by the Discrete Wave Number, *Kovove Mater.*, 50, 221-227.

Hamamoto T., Takahashi H., Tanaka Y., 1991, Stochastic responses of anchored flexible floating islands subjected to wind-waves and seaquakes, *Proceedings of the First International Offshore and Polar Engineering Conference,* 391-398.

Higo Y., 1997, Theoretical study on the effect of seaquakes on a two-dimensional floating body, *Proceedings of the International Offshore and Polar Engineering Conference,* 4, 480-484.

Huerta-Lopez C., Pulliam J., Nakamura Y., 2003, In situ evaluation of shear-wave velocities in seafloor sediments with a broadband ocean-bottom seismograph, Bull. Seism. Soc. Am., 93, 139-151.

Huerta-Lopez C.I., Stokoe II K.H., Valle-Molina C., Pulliam J., Roesset J,M., 2005, Modeling of Seafloor Soft Marine Sediments and Spectral Characteristics of Earthquakes Recorded on the Gulf of Mexico, *J. Offshore Mech. Arct. Eng.*, 127, 1-9.

Hwang I.T., Ting K., 1989, Boundary element method for fluid-structure interaction problems in liquid storage tanks, *J. Pressure Vessel Technol., Transactions of the ASME*, 111, 435-440.

Jang R.D., Higo Y., 2004, A study on seaquake forces acting on floating body due to seaquake by three dimensional time domain analysis, *Proceedings of the International Offshore and Polar Engineering Conference*, 492-496.

Kawase H., 1988, Time-domain response of a semicircular canyon for incident SV, P, and Rayleigh waves calculated by the discrete wave number boundary element method, *Bull. Seism. Soc. Am*., 78, 1415-1437.

Mangano G., D'Alessandro A., D'Anna G., 2011, Long term underwater monitoring of seismic areas: Design of an ocean bottom

seismometer with hydrophone and its performance evaluation, *OCEANS 2011 IEEE* – Spain.

Qian Z.H., 2012, An efficient approach for simulating seismoacoustic scattering due to an irregular fluid-solid interface in multilayered media, *J. Pressure Vessel Technol., Transactions of the ASME,* 189, 524-540.

Rodríguez-Castellanos A., Luzón F., Sánchez-Sesma F.J., 2005, Diffraction of seismic waves in an elastic cracked half-plane using a boundary integral formulation, *Soil Dyn. Earthq. Eng*., 25, 827–837.

Rodríguez-Castellanos A., Flores E., Sánchez-Sesma F.J., Ortiz-Alemán C., Nava-Flores M., Martin R., 2011, Indirect boundary element method applied to fluid-solid interfaces, *Soil Dyn. Earthq. Eng.*, 31, 470-477.

Rodríguez-Castellanos A., Martínez-Calzada V., Rodríguez-Sánchez J.E., Orozco-del-Castillo M., Carbajal-Romero M., 2014, Induced water pressure profiles due to seismic motions, *App. Ocean Res.,* 47, 9-16.

Roever W.L., Vining T.F., Strick E., 1959, Propagation of elastic waves motion from an impulsive source along a fluid/solid interface, *Philosophical Transactions of the Royal Society of London. Series A, Math. Phys. Sci.*, 251, 455-523.

Sánchez-Sesma F.J., Campillo M., 1991, Diffraction of P, SV and Rayleigh waves by topographic features; a boundary integral formulation, *Bull. Seism. Soc. Am*., 81, 1-20.

Schanz M., 2001, Application of 3D time domain boundary element formulation to wave propagation in poroelastic solids, *Eng. Anal. Bound. Elem.*, 25, 363-376.

Tadeu A., Santos J.B., Paulo F.A., 2001, 3-D wave propagation in fluid-filled irregular boreholes in elastic formations, *Soil Dyn. Earthq. Eng*., 21, 499-517.

Takamura H., Masuda K., Maeda H., Bessho M., 2003, A study on the estimation of the seaquake response of a floating structure considering the characteristics of seismic wave propagation in the ground and the water, *J. Mar. Sci. Tech.*, 7, 164-174.

Tanaka Y., Hamamoto T., Kamura H., 1991, Seaquake response of floating circular plates, *Theoret. App. Mechan.*, 40, 81-92.

Trifunac M.D., 1971, Surface motion of a semi-cylindrical alluvial valley for incident plane SH waves, *Bull. Seism. Soc. Am*., 61, 1755-1770.

Trifunac M.D., 1973, Scattering of plane SH waves by a semi-cylindrical canyon, *Earthq. Eng. Struct. D.*, 1, 267-281.

Wade R., 1996, *Practical foundation engineering handbook*, McGraw Hill, New York.

Wong H.L., 1982, Effect of surface topography on the diffraction of P, SV; and Rayleigh waves, *Bull. Seism. Soc. Am*., 72, 1167-1183.